applied sciences

MDPI

Article

Creep Analysis of Rotating Thick Cylinders Subjected to External and Internal Pressure: Analytical and Numerical Approach

Mahir H. Es-Saheb and Yasser Fouad *

Department of Applied Mechanical Engineering, College of Applied Engineering, Muzahimiyah Branch, King Saud University, P.O. Box 800, Riyadh 11421, Saudi Arabia; essaheb@ksu.edu.sa
* Correspondence: yfouad@ksu.edu.sa

Abstract: Creep analysis is crucial when dealing with thick rotating cylinders exposed to a steady load or stress at a higher temperature. These cylinders present a fundamental constituent in a variety of dynamic engineering applications, such as pressure vessels, hydraulic cylinders, gun barrels, boilers, fuel tanks, aerospace technologies, nuclear reactors, and military equipment. Thus, severe mechanical and thermal loads cause significant creep and reduce service life. Hence, the prediction of creep in such axisymmetric components, including pressure vessels, subjected to steady load at elevated temperatures is extremely important and quite a complex task. Thus, in this study, the creep behavior in a rotating thick-walled cylinder made of Al-SiC_p composite subjected to constant load as well as internal and external pressures is investigated, both analytically and numerically, using FEM. A wide range of rotational speeds effect on the process is also included. The creep behavior is assumed to follow the Norton constitutive model, and for stress failure analysis, von Mises yield criteria are adopted. The effect of internal and external pressures, as well as the rotational speed on the stresses, strains, and strain rates in the cylinder, is studied and presented. Both finite element analysis (FEA) and Lame's theory were used to determine the radial, tangential, and longitudinal displacements and corresponding stresses, as well as the equivalent Von Mises stresses and strain rate distributions in the cylinder revolving about its own axis. It is observed that with the increase of the internal pressure in the cylinder, the strain rate increases. Meanwhile, when subjecting the cylinder to both external and internal pressures, the strain rates tend to decrease. For instance, it was also found that stress and strain rates were higher for the 1000 rad/sec rotational speed of thick cylinder in comparison with lower rotational speeds of 300 and 500 rad/sec. Also, it is noticed that the variation in these values at the inner radius was more than those found at the outer radius. All results of the stresses, strains, and strain rate distributions obtained are found to be in full agreement with the published data. Furthermore, all plotted results of the stresses, strains, and strain rate distributions obtained through the analytical approach were found to be in exceptional compliance with those solutions obtained using finite element analysis (FEA).

Keywords: creep; aluminum composite; silicon carbide (Si-C); functionally graded material (FGM); rotating thick cylinders; strain rates; finite element analysis (FEA)

check for updates

Citation: Es-Saheb, M.H.; Fouad, Y. Creep Analysis of Rotating Thick Cylinders Subjected to External and Internal Pressure: Analytical and Numerical Approach. *Appl. Sci.* **2023**, *13*, 11652. https://doi.org/10.3390/app132111652

Academic Editor: José António Correia

Received: 1 September 2023
Revised: 12 October 2023
Accepted: 22 October 2023
Published: 25 October 2023

Copyright: © 2023 by the authors. Licensee MDPI, Basel, Switzerland. This article is an open access article distributed under the terms and conditions of the Creative Commons Attribution (CC BY) license (https://creativecommons.org/licenses/by/4.0/).

1. Introduction

Creep analysis is crucial when dealing with thick rotating cylinders, particularly in high-temperature environments or under sustained loads [1–3]. Thus, the study of creep in these components at a certain rotational speed is important due to their use as a structural component in many engineering applications. In the context of thick rotating cylinders, such as those found in industrial equipment like steam turbines or power generation systems, creep analysis holds significant importance [4,5]. A cylindrical vessel is more likely to serve as the fundamental constituent in a variety of applications, such as pressure

vessels, aerospace technologies, nuclear reactors, and military equipment [6–8]. Creep analysis helps determine the long-term structural integrity of these cylinders by predicting the extent of deformation and the potential for failure over time. By understanding how the material behaves under sustained loads and elevated temperatures, engineers can estimate how long the cylinder can operate safely before reaching a critical level of deformation [9–11]. Creep analysis allows engineers to select material that can withstand operating condition and also permit engineer to schedule effective maintenance [12]. Most engineering applications involve thick cylinders subjected to severe loadings, including both mechanical and thermal, which may result in considerable creep and ultimately reduce its operational life. Therefore, creep forecasting in multiple axisymmetric sections, including pressure vessels, is of prime importance, but it is quite a complex task [13]. Finite element analysis (FEA) is a powerful tool for predicting creep behavior in thick cylinders. It also comes with certain limitations like mesh sensitivity, convergence issues, creep anisotropy, temperature gradient, creep fatigue interaction, and model calibration [14–16]. Hence, the most elaborate finite element procedure yields results that are time-consuming and are not always reliable without verifying.

The cylinder under consideration for creep behavior investigation is assumed to be composed of monolithic material in different studies [17–21]. Mostly, aluminum or its alloys are used in many engineering applications to save power from their lightweight nature, but they are susceptible to creep, which may obstruct their use in large-scale applications [22–24]. It is observed through empirical findings that creep during uniaxial loading can be reduced through the combination of aluminum alloys reinforced with ceramics, i.e., silicon carbide (Si-C) in comparison with pure aluminum [25–28]. It may impart considerable strength to composites (combination of aluminum alloys with ceramics) [29–31]. Ziaei et al. [32] examined the stress redistribution along with creep in a thick-walled cylinder composed of functionally graded material (FGM) subjected to heat flux and mechanical loading through the Baily Norton model. They found maximum circumferential and radial strain rates at the inner surface of the FGM vessel. Tensile stress usually travels from the high-stress areas to the areas that possess lower strain rates during creep strain propagation. For thick-walled FGM cylinders, the higher order Taylor series provides creep stress and strain results more accurately, while lower order Taylor series produce more accurate creep stress/strain results in thin-walled cylinder. Arya [19] studied anisotropy impact on strain creep behavior in the thick-walled composite cylinder and observed that anisotropy positively impacts the reduction in the stress, strains, and strain-rates values in comparison with corresponding values for an isotropic material and results in a longer lifespan.

Temesgen et al. [33] applied Seth transition and generalized strain measure theory in order to derive the creep transition stresses/strain rates in a spherical shell composed of isotropic or transversely isotropic materials under uniform pressure and thermal gradient. They found that circumferential stress/strain rates in the case of isotropic material are higher than for transversely isotropic material under high-temperature conditions at the internal surface. However, the pressure vessel made up of transversely isotropic material is considered safe under high temperature/pressure applications as compared to a pressure vessel composed of isotropic material. Batra [34] considered hollow FGM cylinders for axisymmetric plane strain radial under the application of uniform hydrostatic pressures. The cylinder was supposed to be composed of isotropic/incompressible linear elastic material. He observed optimal hoop/circumferential stress value for the linear variation in a radial direction of shear modulus. Benslimane et al. [35] validated the accuracy of the analytical solution through a numerical model (FEM). Chamoli et al. [36] compared von Mises and Tresca yielding criteria in order to investigate the impact of anisotropy on creep behavior and of a rotating disc composed of composite material (aluminum-silicon carbide). They found the Tresca criterion more accurate than the von Mises criterion as the results obtained through the Tresca criterion are much closer to empirical values. Nie et al. [37] found volume fractions of linear elastic hollow cylinders and spheres composed

of FGM vary only with the radius. After reviewing a tremendous amount of the literature, the current study is designed to ascertain the steady state creep in a rotating cylinder made of Al-SiC composite under thermos-mechanical loading using Tresca and von Mises yield criteria. A mathematical model based on Sherby's threshold stress-based law was also established to portray the steady state creep behavior of composite cylinders [38].

In this study, the above issues are discussed, and the creep behavior in a rotating thick-walled cylinder made of Al-SiC_p composite subjected to constant load as well as internal and external pressures is investigated. Solutions to the problem utilizing both analytical and numerical techniques using FEM are developed and presented. A wide range of rotational speed effects on the process is also explored. In the analysis, the creep behavior is assumed to follow the Norton constitutive model, and von Mises yield criteria for stress failure analysis are employed. The effect of internal and external pressures, as well as the rotational speed on the stresses, strains, and strain rates in the thick cylinder, is studied and presented. Both finite element analysis (FEA) and Lame's theory are used to calculate the radial, tangential, and longitudinal displacements and corresponding stresses, as well as the equivalent Von Mises stresses and strain rate distributions in the cylinder revolving about its own axis. The FEA results will be validated, and all obtained results accuracy will be examined for compliance with published data.

2. Mathematical Formulation

2.1. Analytical Analysis

Complete general detailed analytical solution and creep analysis for the rotating thick cylinder subjected to internal and external pressures is derived and presented. The solution is based on the well-documented Lame's theoretical approach. In this analysis, a thick-walled axisymmetric cylinder with inner and outer radii of r_{in}, and r_{out}, under internal and external pressures P_{in} and P_{out} rotating about its own axis with constant angular velocity ω considered. It is made of Al-SiC_p composite, and ρ is the material density. For the sake of analysis, in the current study, few assumptions have been made. These are:

(i) Incompressible and isotropic cylinder material with uniform distribution of silicon carbide in aluminum matrix.
(ii) Gradual increase in applied pressure but remains constant during loading history.
(iii) Steady-state condition of stress at any point in the cylinder.
(iv) Small elastic deformations can be neglected in comparison with creep deformations.

However, a brief account of derivation and a summary of the main governing equations and formulations used in the study, together with the conditions applied, are given in the next sections.

The equilibrium equation is given as

$$\frac{\delta\sigma_r(r)}{\delta r} + \frac{\sigma_r(r) - \sigma_t(r)}{r} + \rho\omega^2 r = 0 \tag{1}$$

where $\sigma_r(r)$ and $\sigma_t(r)$ represent stresses in the respective directions.

As the creep deformations do not undergo considerable volume changes, one may write.

$$\dot{\varepsilon}_r + \dot{\varepsilon}_t + \dot{\varepsilon}_z = 0 \tag{2}$$

where $\dot{\varepsilon}_r$, $\dot{\varepsilon}_t$ and $\dot{\varepsilon}_z$ are the strain rates in the radial, transverse, and z-axis, respectively.

It is assumed that the condition of plain strain prevails as a cylinder is inhibited from contracting axially. Therefore,

$$\dot{\varepsilon}_z = 0 \tag{3}$$

Solving Equations (2) and (3) result in Equation (4)

$$\dot{\varepsilon}_r = -\dot{\varepsilon}_t \tag{4}$$

For cylinder material creep behavior, it is assumed to follow the Norton Equation, given as

$$\dot{\varepsilon}_e = B{\sigma_e}^n \tag{5}$$

where, σ_e is effective stress, $\dot{\varepsilon}_e$ is effective strain rate subjected to multi-axial stress, B and n are creep constants of materials.

The generalized constitutive creep equations for the isotropic composite are:

$$\dot{\varepsilon}_r = \frac{\dot{\varepsilon}_e}{\sigma_e}\left(\sigma_r - \frac{1}{2}(\sigma_t + \sigma_z)\right) \tag{6}$$

$$\dot{\varepsilon}_t = \frac{\dot{\varepsilon}_e}{\sigma_e}\left(\sigma_t - \frac{1}{2}(\sigma_r + \sigma_z)\right) \tag{7}$$

$$\dot{\varepsilon}_z = \frac{\dot{\varepsilon}_e}{\sigma_e}\left(\sigma_z - \frac{1}{2}(\sigma_r + \sigma_t)\right) \tag{8}$$

2.2. Von Mises Criterion

The effective stress, as shown in Equation (5), is evaluated by substituting the state of stresses obtained into Von Mises criterion, as follows:

$$\sigma_e = \frac{1}{\sqrt{2}}\left[(\sigma_t - \sigma_r)^2 + (\sigma_r - \sigma_z)^2 + (\sigma_z - \sigma_t)^2\right]^{1/2} \tag{9}$$

Substituting Equation (3) into Equation (8) results in axial stress,

$$\sigma_z = 0.5(\sigma_r + \sigma_t) \tag{10}$$

Using this value of σ_z in Equations (6) and (7), one gets,

$$\dot{\varepsilon}_r = \frac{3}{4}\frac{\dot{\varepsilon}_e}{\sigma_e}(\sigma_r - \sigma_t) \tag{11}$$

and Equation (7) becomes.

$$\dot{\varepsilon}_t = -\frac{3}{4}\frac{\dot{\varepsilon}_e}{\sigma_e}(\sigma_r - \sigma_t) \tag{12}$$

Using Equation (10) in Equation (9),

$$\sigma_e = \frac{\sqrt{3}}{2}(\sigma_t - \sigma_r) \tag{13}$$

The strain rates in radial and tangential directions are represented through Equations (14) and (15), with u is the radial displacement at any radius r,

$$\dot{\varepsilon}_r = \frac{\delta \dot{u}}{\delta r} \tag{14}$$

$$\dot{\varepsilon}_t = \frac{\dot{u}}{r} \tag{15}$$

Eliminating $\dot{u}$ from Equations (14) and (15), one gets,

$$r\frac{\delta \dot{\varepsilon}_t}{\delta r} + \dot{\varepsilon}_t - \dot{\varepsilon}_r = 0 \tag{16}$$

Using Equations (11) and (12), in Equation (16), one gets,

$$nr\left(\frac{\delta \sigma_t}{\delta r} - \frac{\delta \sigma_r}{\delta r}\right) + 2(\sigma_t - \sigma_r) = 0 \tag{17}$$

Eliminating σ_t from Equations (1) and (17), one gets,

$$nr^2\frac{\delta^2\sigma_r}{\delta r^2} + 2r\sigma_r + 2\rho r^2\omega^2(n+1) = 0 \tag{18}$$

Solving the differential Equation (18), which is a Cauchy-Euler Equation, we get.

$$\sigma_r = -\frac{\rho\omega^2}{2}r^2 + C_1 + C_2 r^{\frac{-2}{n}} \tag{19}$$

where, C_1 and C_2 are constants determined from the boundary condition of the problem.

Substituting Equation (19) in Equation (17), one gets,

$$\sigma_t = -\frac{\rho\omega^2}{2}r^2 + C_1 + \left(\frac{n-2}{n}\right)C_2 r^{\frac{-2}{n}} \tag{20}$$

Then substituting Equations (19) and (20) in Equation (10)

$$\sigma_z = -\frac{\rho\omega^2}{2}r^2 + C_1 + \left(\frac{n-1}{n}\right)C_2 r^{\frac{-2}{n}} \tag{21}$$

3. Numerical Analysis and FEA Model

As stated above, a comprehensive stress analysis is carried out on a thick-walled rotating cylinder made of Al-SiC_p composite using both analytical and numerical methods. However, for the purpose of analysis and the implementation and validation of the formulated equations derived and to display some typical presentable numerical values and results, some typical values for the investigated parameters, dimensions, materials properties, pressure conditions, etc., are assigned. The typical depicted values used in the study are: cylinder material is made of Al-SiC_p composite containing 10 vol.% of SiC_p, Inner radius: r_{in} = 300 mm, Outer radius: r_{out} = 450 mm, n = 1, $B = 1.0 \times 10^{-85}\left(\mathrm{m}^2/\mathrm{N}\right)^n$, ρ = 2900 kg/m^3, P_{in} = 60 Mpa, P_{out} = 40 Mpa. The rotational speeds of 300, 500, and 1000 rad/sec were also depicted to display typical sample results.

However, for the FEA method, a cylinder is modeled and meshed by an axisymmetric element (PLANE183 2D Structural Solid) in ANSYS® [39], as shown in Figures 1 and 2. Also, boundary conditions for the cylinder are free in the x-direction and fixed in the y-direction at both ends.

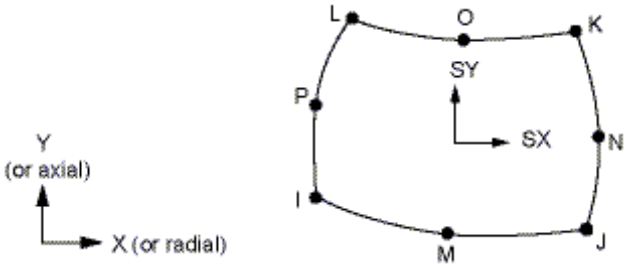


Figure 1. PLANE183(Quadrilateral) Geometry.

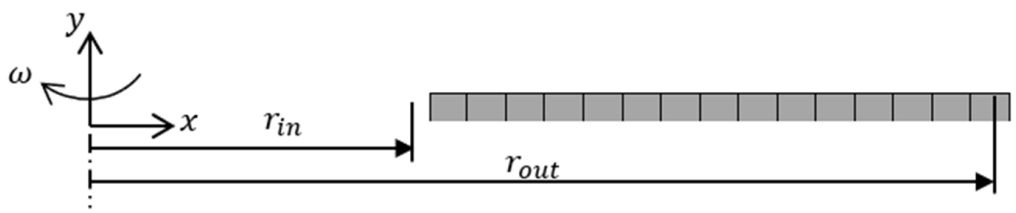


Figure 2. Cross-section of cylinder section meshed by 15 axisymmetric elements.

It is important to state that, to get and extract the values of the equivalent creep strain, which is the independent dominant variable in the model, we have to determine first the equivalent creep strain and then apply it in the constitutive model (Norton Equation) to get the Von-Mises stress, and consequently substituting these values in material properties laws, all strains and strain rates will be attained. At this stage, it is recognized that the model analysis time is the main factor that affects the equivalent creep strain, and this time is greatly influenced by rotational velocity ω. Therefore, to identify the proper time model to be used to determine strain rate values, a series of trial-and-error tests to establish the relation between rotational velocity ω and analysis time has to be conducted, as can be seen in Figure 3.

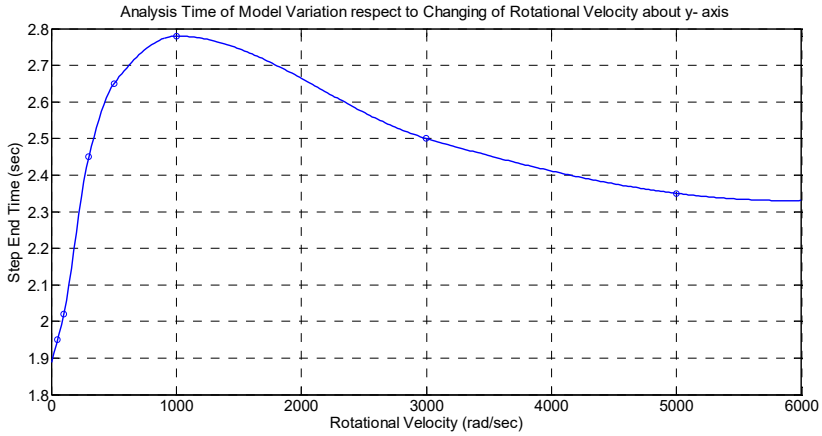
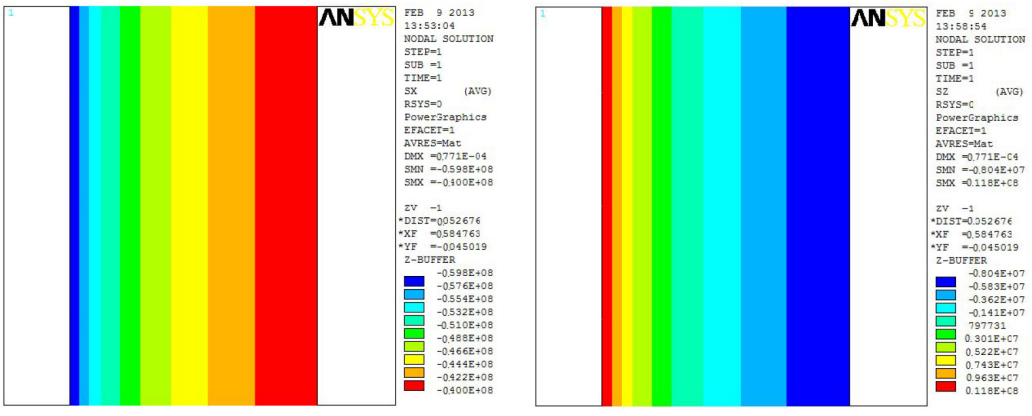


Figure 3. Analysis time versus rotational velocity ω.

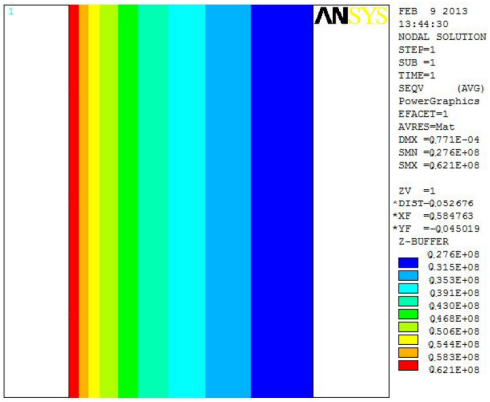
4. Analytical and Numerical Solutions

Applying analytical, numerical, and FE ANSYS® solutions, vast results of radial, tangential, Von-Mises stresses, and strain rates for all loadings and rotational speed conditions are obtained. However, as stated above, the depicted speeds used for calculations and result display were 300, 500, and 1000 rad/sec. Typical FE results obtained for radial stress σ_r; tangential stress σ_t; and equivalent Von Mises Stress σ_e in the radial direction are shown on part of the cylinder color contour graphs in Figure 4, for $\omega = 300$ rad/sec. Meanwhile, Figures 5–8 show the radial stress, tangential stress, axial stress, and equivalent Von-Mises stress obtained from both analytical and numerical solutions for the three rotational speeds 300, 500, and 1000 rad/sec, respectively. All results shown are in full agreement with similar published data and display excellent compliance and high accuracy between analytical and numerical solutions [31–34,40–43].



(**a**) (**b**)

Figure 4. *Cont.*



(**c**)

Figure 4. Variation of (**a**) Radial Stress σ_r; (**b**) Tangential Stress σ_t; (**c**) Equivalent Von Mises in the radial direction Stress σ_e, for $\omega = 300$ rad/sec.

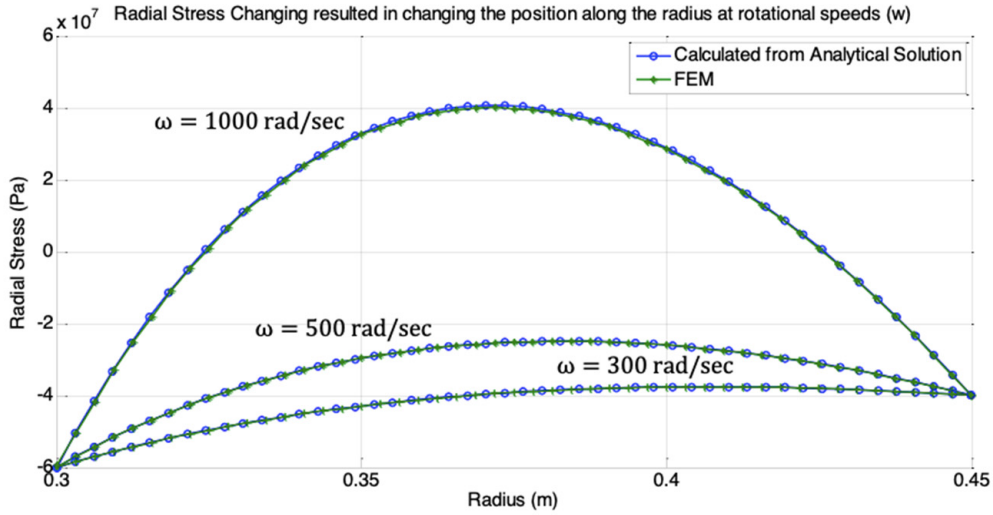


Figure 5. Variation of Radial Stress σ_r in the radial direction Stress of cylinder.

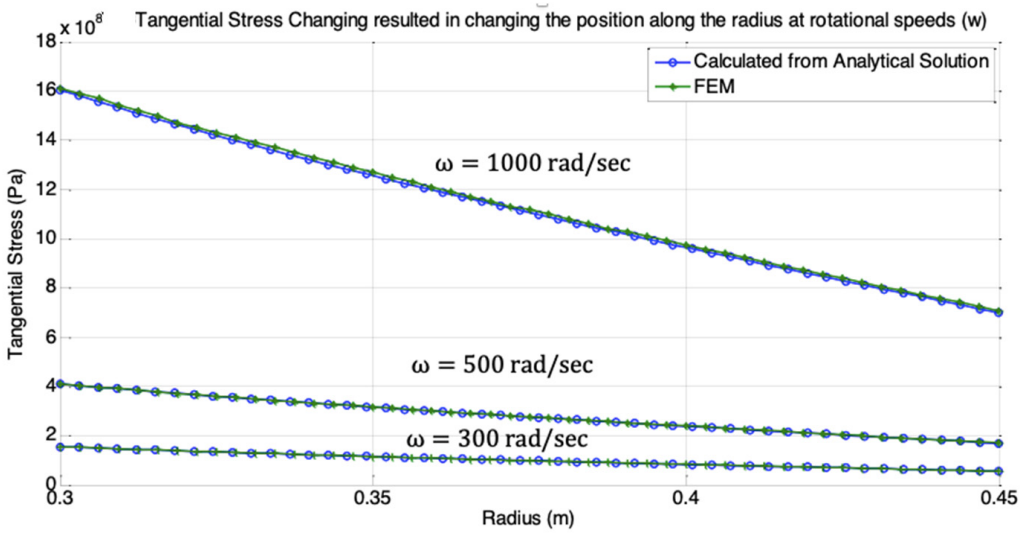


Figure 6. Variation of Radial Stress σ_t in the radial direction Stress of cylinder.

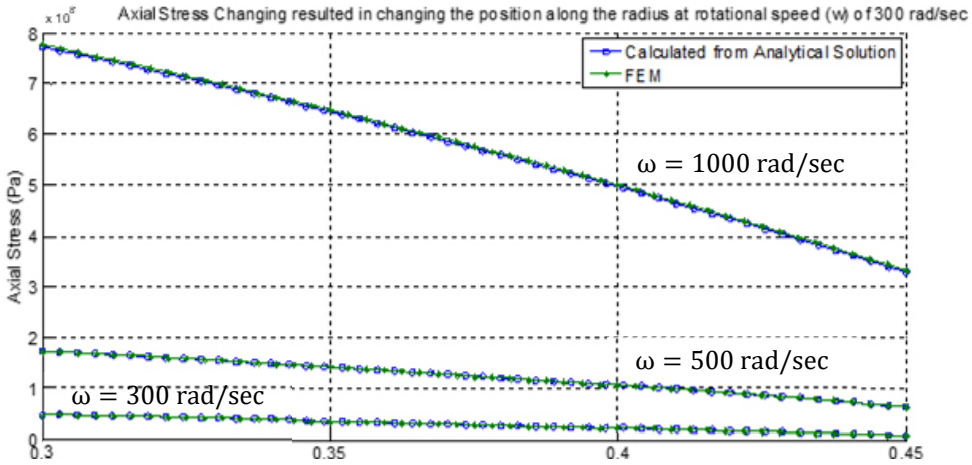


Figure 7. Variation of Axial Stress σ_z in the radial direction Stress of cylinder.

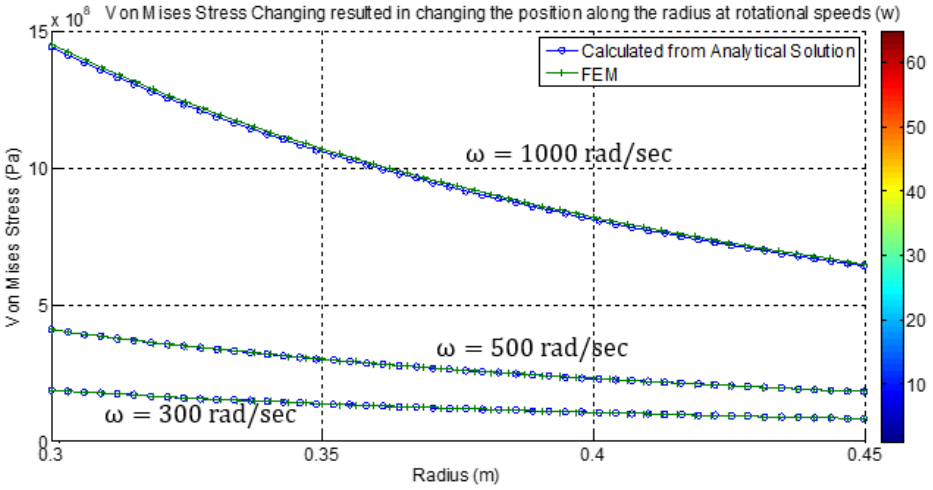


Figure 8. Variation of Von Mises Stress σ_e in the radial direction of the cylinder.

Finally, Figures 9–11 show the radial strain rate, tangential strain rate, and equivalent creep strain obtained from both analytical and numerical solutions for the three rotational speeds 300, 500, and 1000 rad/sec, respectively. Again, all results shown are in full agreement with similar published data and display excellent compliance and high accuracy between analytical and numerical solutions [26–29,40–43].

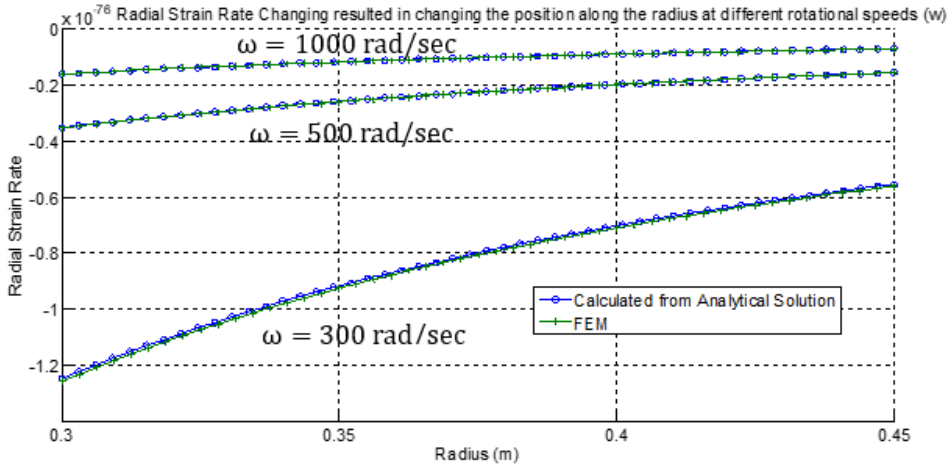


Figure 9. Variation of Radial Strain Rate $\dot{\varepsilon}_r$ in the radial direction of the cylinder.

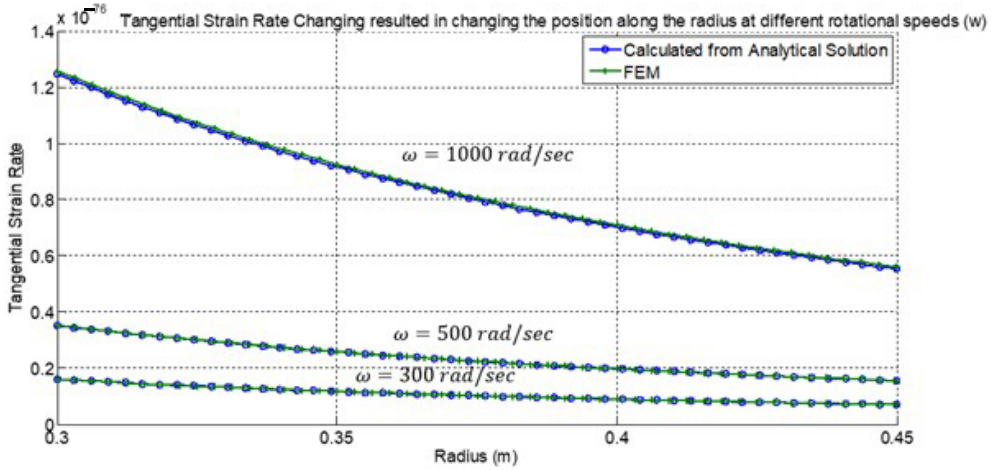


Figure 10. Variation of Tangential Strain Rate $\dot{\varepsilon}_t$ in the radial direction of the cylinder.

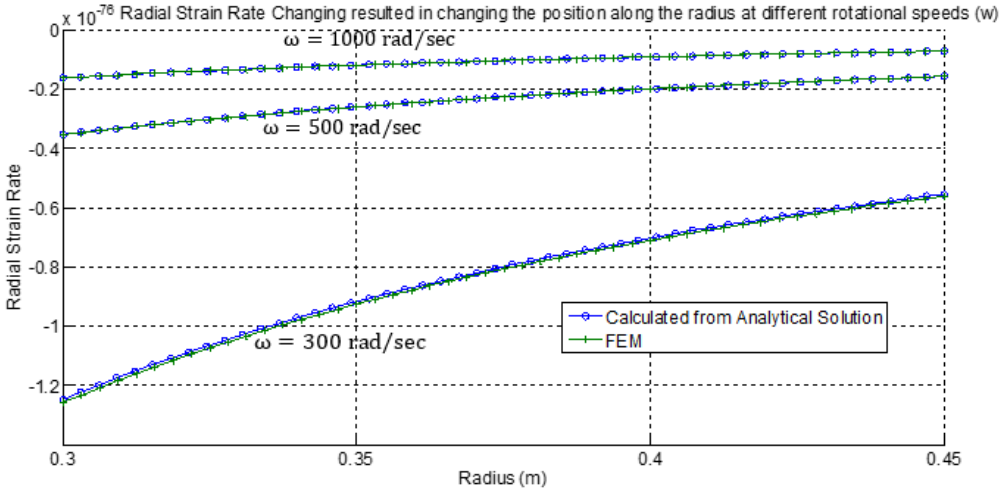


Figure 11. Variation of Equivalent Creep Strain Rate $\dot{\varepsilon}_e$ in the radial direction of the cylinder.

In Figure 5, trends of radial stresses σ_r distribution obtained from analytical and numerical solutions are shown in the radial direction of the cylinder for $\omega = 300$, $\omega = 500$, and $\omega = 1000$ rad/sec. These stresses remain constant both at the outer and inner surfaces. However, they possess maximum values for radius $r \cong (r_{in} + r_{out})/2$ for $\omega = 300$, $\omega = 500$, and $\omega = 1000$ rad/sec. But they increase gradually with an increase in the rotational velocity ω.

Figure 6 depicts the trends in tangential stresses σ_t acquired through analytical and numerical approach radially through cylinder for $\omega = 300$, $\omega = 500$, and $\omega = 1000$ rad/sec. The tangential stresses decline gradually at the outer periphery of the cylinder while minutely increasing at the inner periphery of the cylinder as the rotational velocity ω increases. The tangential stresses are higher at the inner periphery of the cylinder than at the outer periphery. As seen from Figure 6 these stresses become nearly constant radially through the cylinder for $\omega = 300$ rad/sec and low rotational velocities.

Figure 7 depicts the trends in axial stresses σ_z acquired through analytical and numerical approach radially through cylinder for $\omega = 300$, $\omega = 500$, and $\omega = 1000$ rad/sec. The axial stresses decline gradually at the outer periphery of the cylinder while minutely increasing at the inner periphery of the cylinder as the rotational velocity ω increases. The tangential stresses are higher at the inner periphery of the cylinder than at the outer periphery. As seen from Figure 7 these stresses become nearly constant radially through the cylinder for $\omega = 300$ rad/sec and low rotational velocities.

Figure 8 represents the trends of Von Mises stresses σ_e acquired through analytical and numerical approach radially through cylinder for $\omega = 300$, $\omega = 500$, and $\omega = 1000$ rad/sec. The Von Mises stresses decline gradually at the outer periphery of the cylinder while minutely increasing at the inner periphery of the cylinder as the rotational velocity ω increases. The Von Mises stresses are higher at the inner periphery of the cylinder than at the outer periphery. As seen from Figure 8 these stresses become nearly constant radially through the cylinder for $\omega = 300$ rad/sec and low rotational velocities.

Figure 9 represents the trends of radial strain rates $\dot{\varepsilon}_r$ radially through cylinder for $\omega = 300$, $\omega = 500$, and $\omega = 1000$ rad/sec. All radial strain rates are higher (in magnitude) at the inner periphery of the cylinder and vary with parallel curves radially through the cylinder. It can be observed from Figure 9 that radial strain rate increase is potentially much higher at lower rotational speed, as can be seen from its trend line with maximum difference between initial and final values. In a pressurized cylinder, the internal or external pressure creates hoop stresses, which are tangential stresses along the circumference of the cylinder. These hoop stresses generate forces that cause radial expansion of the cylinder's cross-section. As we move from the inner radius to the outer radius, the magnitude of the hoop stress decreases due to the principles of mechanics [39].

Figure 10 shows variations of tangential strain rates $\dot{\varepsilon}_t$ radially through cylinder for $\omega = 300$, $\omega = 500$, and $\omega = 1000$ rad/sec. All tangential strain rates are higher (in magnitude) at the inner periphery of the cylinder and vary with parallel curves radially through the cylinder. The tangential strain rates decrease progressively as rotational velocity increases. The percent decrease in tangential strain rate is higher for 1000 rad/sec rotational speed in comparison to lower rotational speeds. Moreover, the results show reasonable compliance between FEM and analytical solutions. When internal pressure is applied to a thick-walled cylinder, the pressure generates hoop stresses (tangential stresses) along the circumference of the cylinder. At smaller radii (closer to the inside surface), the material experiences a higher internal pressure, resulting in higher hoop stresses. For larger radii (closer to the outside surface), the internal pressure acting on the material decreases, leading to lower hoop stresses [40].

It is important to state that in creep modeling, it is common to attain or encounter very high exponential coefficients. In some cases, the noticed value could reach about 10 power -90, especially in cases where the material investigated is relatively brittle, the values of strain are extremely small, and the load time history covers a very long period of time, as happened in our case, but in general, when dealing with normal materials and shorter periods of load time history, the average reported values are around 10 power -13 [9,15,16,43].

Figure 11 shows variations of equivalent creep strain rates $\dot{\varepsilon}_e$ radially through cylinder for $\omega = 300$, $\omega = 500$, and $\omega = 1000$ rad/sec. All equivalent creep strain rates are higher (in magnitude) at the inner periphery of the cylinder and vary with parallel curves radially through the cylinder. They decrease gradually as rotational velocity increases.

Finally, Figure 12 displays the linear trend of varying equivalent creep strain with respect to time in this time region at all different radii of the cylinder. Because of using the Norton Constitutive model, which is valid in secondary creep region only (linear region behavior), the figure above can be explained. The equivalent creep strain is maximum for a lower radius (0.3 m) and decreases as the radius increases from 0.3 to 0.45 m. It can be credited to higher stress concentration at lower radius. Moreover, in regions with lower radii, the material might experience more pronounced microstructural alterations, which can influence the creep behavior and lead to a higher creep strain rate [41,42].

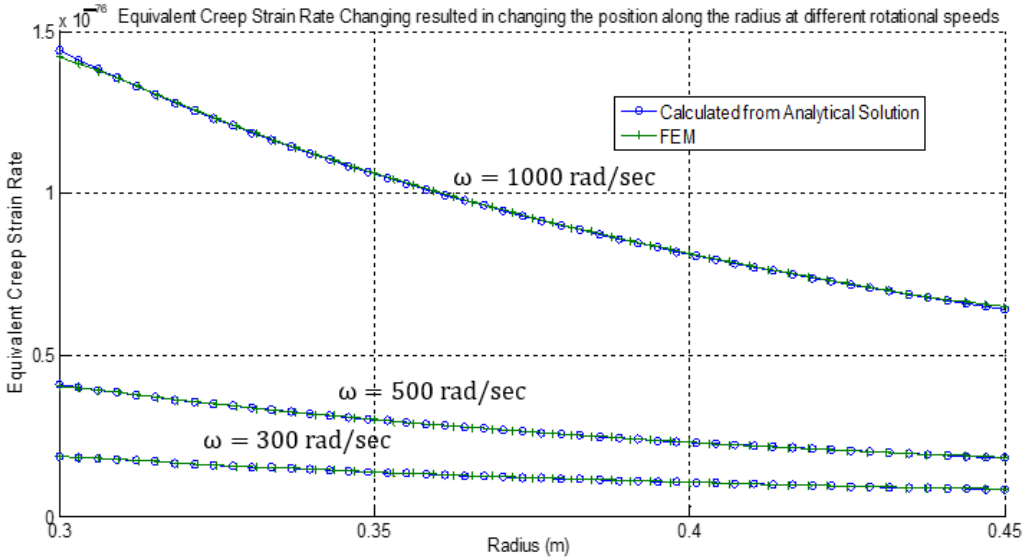


Figure 12. Variation of Equivalent Creep Strain Rate $\dot{\varepsilon}_e$ with respect to time at different radii.

5. Conclusions

A few main conclusions can be drawn from the current study. These can be summarized as:

- Analytical and numerical solutions, using FEA, of the creep problem in rotating thick cylinders made of Al-SiC_p composite and subjected to internal and external pressures were successfully achieved.
- All results of the stresses, strains, and strain rates distributions obtained are found to be in full agreement with the published data.
- All plotted results of the stresses, strains, and strain rate distributions obtained through the analytical approach were found to be in excellent compliance with those solutions obtained using finite element analysis (FEA).
- FEA Model was verified through a calculated model from exact analytical analysis.
- The radial stresses σ_r obtained from analytical and numerical solutions are constant at the inner and outer surfaces, but they are higher at radius $r \cong (r_{in} + r_{out})/2$ for $\omega = 300$, $\omega = 500$, and $\omega = 1000$ rad/sec.
- The radial stresses σ_r obtained from analytical and numerical solutions, increase gradually with an increase in the rotational velocity ω.
- The variations of tangential stresses σ_t decrease gradually at the outer surface and increase very little at the inner surface with increasing rotational velocity ω.
- The tangential stresses σ_t are also higher at the inner surface than those at the outer surface.
- Tangential stresses attained nearly constant values in the radial direction of the cylinder for ω = 300 rad/sec and low rotational velocities.
- Variations of Axial stresses σ_z have the same behavior as tangential stresses σ_t.
- All radial strain rate values are higher (in magnitude) at the inner surface and vary with parallel curves in the radial direction of the cylinder.
- All radial strain rates decrease gradually with an increase in the rotational velocity.
- All tangential strain rates and equivalent creep strain rates have the same behavior as radial strain rates.

Author Contributions: Conceptualization, M.H.E.-S.; Methodology, Y.F.; Software, M.H.E.-S.; Validation, Y.F.; Investigation, Y.F.; Resources, M.H.E.-S.; Data curation, M.H.E.-S.; Writing—original draft, M.H.E.-S.; Writing—review & editing, Y.F.; Visualization, M.H.E.-S.; Project administration, Y.F.; Funding acquisition, Y.F. All authors have read and agreed to the published version of the manuscript.

Funding: The authors extend their appreciation to the Researchers Supporting Project number (RSPD2023R698), King Saud University, Riyadh, Saudi Arabia, for funding this research work.

Institutional Review Board Statement: Not applicable.

Informed Consent Statement: Not applicable.

Data Availability Statement: The datasets generated during and/or analyzed during the current study are available from the corrsponding author on reasonable request.

Conflicts of Interest: The authors declare no conflict of interest.

Nomenclature

FEA/M	Finite Element Analysis/Method
FGM	Functionally Graded Material
(Si-C)	Silicon Carbide
Al-SiC_p	Aluminum Silicon Carbide composite
r_{in}	Inner radius
r_{out}	Outer radius
P_{in}	Internal pressure
P_{out}	External pressure
ρ	Material density
ω ras/sec	Angular/Rotational velocity
$\sigma_r(r)$	Radial stress
$\sigma_t(r)$	Tangential stress
σ_z	Axial stress
$\dot{\varepsilon}_r$	Radial strain rate
$\dot{\varepsilon}_t$	Tangential strain rate
$\dot{\varepsilon}_z$	Axial strain rate
σ_e	effective stress
$\dot{\varepsilon}_e$	Effective strain rate
B and n	Creep materials constants
u	Radial displacement
C_1 and C_2	Boundary constants

References

1. Arya, V. Large strain creep analysis of composite thick-walled anisotropic cylinders. *J. Mech. Eng. Sci.* **2023**, *17*, 9395–9409. [CrossRef]
2. Bhatta, L.; Pesin, A.; Zhilyaev, A.P.; Tandon, P.; Kong, C.; Yu, H. Recent Development of Superplasticity in Aluminum Alloys: A Review. *Metals* **2020**, *10*, 77. [CrossRef]
3. Zheng, J.-H.; Jin, Y.; Xu, L.; Fan, C.; Song, W.; Chen, Y. Comparative Study of Creep and Stress Relaxation Behaviour during Ageing of 7050 Aluminum Alloy. *Metals* **2023**, *13*, 778. [CrossRef]
4. Abdulsahib, A.D.; Al-Farhany, K. Review of the Effects of Stationary/Rotating Cylinder in a Cavity on the Convection Heat Transfer in Porous Media with/without Nanofluid. *Math. Model. Eng. Probl.* **2021**, *8*, 356–364. [CrossRef]
5. Lao, S.; Zhan, L.; Qian, W.; Xu, Y.; Ma, B.; Liu, C.; Huang, M.; Yang, Y.; Chen, K.; Peng, N.; et al. Creep Aging Behavior of a Thermo-Mechanical Treated 7B04 Aluminum Alloy. *Metals* **2023**, *13*, 182. [CrossRef]
6. Azeem, M.; Ya, H.H.; Alam, M.A.; Kumar, M.; Stabla, P.; Smolnicki, M.; Gemi, L.; Khan, R.; Ahmed, T.; Ma, Q.; et al. Application of Filament Winding Technology in Composite Pressure Vessels and Challenges: A Review. *J. Energy Storage* **2022**, *49*, 103468. [CrossRef]
7. Jayaraman, P.; Pandey, A. Mechanical Design and Analysis of CNT Modified Carbon Fibre Composite Pressure Vessel. In Proceedings of the AIAA AVIATION 2022 Forum, Chicago, IL, USA, 27 June–1 July 2022.
8. Heugue, P.; Larouche, D.; Breton, F.; Martinez, R.; Chen, X.-G.; Massinon, D. Modelling of Strain-Controlled Thermome-chanical Fatigue Testing of Cast $AlSi_7Cu_{3.5}Mg_{0.15}$ (Mn, Zr, V) Alloy for Different Aging Conditions. *Metals* **2022**, *12*, 1258. [CrossRef]
9. Smaisim, G.F.; Bidgoli, M.O.; Goh, K.L.; Bakhtiari, H. Review of thermoelastic, thermal properties and creep analysis of functionally graded cylindrical shell. *Aust. J. Mech. Eng.* **2022**, 1–12. [CrossRef]
10. Orozco-Caballero, A.; Álvarez-Leal, M.; Carreño, F.; Ruano, O.A. Superplastic Behavior of Overaged 2024 Aluminum Alloy after Friction Stir Processing. *Metals* **2022**, *12*, 1880. [CrossRef]
11. Qiao, K.; Zhu, A.; Wang, B.; Di, C.; Yu, J.; Zhu, B. Characteristics of Heat Resistant Aluminum Alloy Composite Core Conductor Used in overhead Power Transmission Lines. *Materials* **2020**, *13*, 1592. [CrossRef]

12. Sahni, M.; Mehta, P.D.; Sahni, R.; León-Castro, E.; Espinoza-Audelo, L.F. Secondary Creep Analysis of FG Rotating Cylinder with Exponential, Linear and Quadratic Volume Reinforcement. *Materials* **2022**, *15*, 1803. [CrossRef] [PubMed]
13. Zhang, X.-C.; Gong, J.-G.; Xuan, F.-Z. A deep learning based life prediction method for components under creep, fatigue and creep-fatigue conditions. *Int. J. Fatigue* **2021**, *148*, 106236. [CrossRef]
14. Almeida, J.H.S.; Lisbôa, T.V.; Spickenheuer, A.; St-Pierre, L. A sequential finite element model updating routine to identify creep parameters for filament wound composite cylinders in aggressive environments. *Comput. Struct.* **2023**, *276*, 106939. [CrossRef]
15. Liu, Y.; Wang, Y.; Wei, D.; Jiang, X.; Tao, Q. Modeling of Creep Deformation Behavior of DZ411 and Finite Element Simulation of Turbine Blade. *Metals* **2023**, *13*, 1389. [CrossRef]
16. Katouzian, M.; Vlase, S.; Scutaru, M.L. Finite Element Method-Based Simulation Creep Behavior of Viscoelastic Carbon-Fiber Composite. *Polymers* **2021**, *13*, 1017. [CrossRef]
17. Bansal, S.; Singh, S.B. Steady-State Creep Deformation In Rotating Discs And Cylinders: For Macro To Micro/Nano-Scale Systems. In *Nanotechnology-Enhanced Solid Materials: Design, Synthesis, Properties, Applications, and Perspectives*; Apple Academic Press: Cambridge, MA, USA, 2023; p. 259. [CrossRef]
18. Bansal, S.; Singh, S.; Haghi, A. Investigations of Flow Behavior in Cylinder and Disc Made of Monolithic and Composite Materials. In *Materials Modeling for Macro to Micro/Nano Scale Systems*; Apple Academic Press: Cambridge, MA, USA, 2022; pp. 269–306.
19. Arya, V.K. Effect of anisotropy on the large strain creep behavior of composite thick-walled spherical vessels. *J. Braz. Soc. Mech. Sci. Eng.* **2022**, *44*, 473. [CrossRef]
20. Madani, K.; Houari, A.; Bouchikhi, A.; Mokhtari, M. Numerical analysis of the elastic-plastic behavior of a tubular structure in FGM under pressure and defect presence. *Frat. Ed Integrità Strutt.* **2022**, *16*, 212–231. [CrossRef]
21. Lei, C.; Li, H.; Fu, J.; Shi, N.; Zheng, G.; Bian, T. Damage in Creep Aging Process of an Al-Zn-Mg-Cu Alloy: Experiments and Modeling. *Metals* **2018**, *8*, 285. [CrossRef]
22. Rakhmonov, J.U.; Bahl, S.; Shyam, A.; Dunand, D.C. Cavitation-resistant intergranular precipitates enhance creep performance of θ′-strengthened Al-Cu based alloys. *Acta Mater.* **2022**, *228*, 117788. [CrossRef]
23. Michi, R.A.; Sisco, K.; Bahl, S.; Yang, Y.; Poplawsky, J.D.; Allard, L.F.; Dehoff, R.R.; Plotkowski, A.; Shyam, A. A creep-resistant additively manufactured Al-Ce-Ni-Mn alloy. *Acta Mater.* **2022**, *227*, 117699. [CrossRef]
24. Yang, Q.; Yan, Z.; Lv, S.; Guan, K.; Qiu, X. Abnormal creep stress exponents in a high-pressure die casting Mg–Al−RE alloy. *Mater. Sci. Eng. A* **2022**, *831*, 142203. [CrossRef]
25. Frankberg, E.J.; Lambai, A.; Zhang, J.; Kalikka, J.; Khakalo, S.; Paladino, B.; Cabrioli, M.; Mathews, N.G.; Salminen, T.; Hokka, M.; et al. Exceptional Microscale Plasticity in Amorphous Aluminum Oxide at Room Temperature. *Adv. Mater.* **2023**, *142*, e2303142. [CrossRef] [PubMed]
26. Zhang, M.; Lewis, R.; Gibeling, J. Mechanisms of creep deformation in a rapidly solidified Al–Fe–V–Si alloy. *Mater. Sci. Eng. A* **2021**, *805*, 140796. [CrossRef]
27. Manjunath, R.; Kumar, D.; Kumar, A. A Review on the Significance of Hybrid Particulate Reinforcements on the Mechanical and Tribological Properties of Stir-Casted Aluminum Metal Matrix Composites. *J. Bio-Tribo-Corros.* **2021**, *7*, 122. [CrossRef]
28. Sohag, A.Z.; Gupta, P.; Kondal, N.; Kumar, D.; Singh, N.; Jamwal, A. Effect of ceramic reinforcement on the microstructural, mechanical and tribological behavior of Al-Cu alloy metal matrix composite. *Mater. Today Proc.* **2020**, *21*, 1407–1411. [CrossRef]
29. Singh, L.; Kumar, S.; Raj, S.; Shivam; Badhani, P. Development and characterization of aluminium silicon carbide composite materials with improved properties. *Mater. Today Proc.* **2021**, *46*, 6733–6736. [CrossRef]
30. Arya, R.K.; Kumar, R.; Telang, A. Influence of Microstructure on Tribological Behaviors of Al6061 Metal Matrix Composite Reinforced with Silicon Nitride (Si_3N_4) and Silicon Carbide (SiC) Micro Particles. *Silicon* **2023**, *15*, 3987–4001. [CrossRef]
31. Gouda, S.; Gouda, S.; Kumar, G.B.V.; Kumar, G.B.V.; Pramod, R.; Pramod, R.; Prasanna, N.D.; Prasanna, N.D.; Balasubramanya, H.S.; Balasubramanya, H.S.; et al. Fabrication, Mechanical and Wear Properties of Aluminum (Al6061)-Silicon Carbide-Graphite Hybrid Metal Matrix Composites. *Frat. Ed Integrità Strutt.* **2022**, *16*, 134–149. [CrossRef]
32. Ziaei-Asl, A.; Saviz, M.R.; Pourabdollah, J. Creep and Stress Redistribution Analysis of Thick-Wall FGM Spheres Subjected to Mechanical Load and Heat Flux–An Analytical Approach. *J. Adv. Mater. Process.* **2020**, *8*, 53–64.
33. Temesgen, A.G.; Singh, S.B.; Pankaj, T. Modeling of Creep Deformation in an Internally Pressurized Transversely Isotropic Spherical Shell Subjected to a Thermal Gradient. *Mech. Solids* **2022**, *57*, 937–948. [CrossRef]
34. Zhang, N.; Lu, A.; Li, C.C.; Zhou, J.; Zhang, X.; Wang, S.; Chen, X.; Mohammadi, M.; Saha, G.; Akbarzadeh, A.; et al. Optimal Design of Functionally Graded Incompressible Linear Elastic Cylinders and Spheres. *AIAA J.* **2008**, *46*, 2050–2057. [CrossRef]
35. Benslimane, A.; Benchallal, R.; Mammeri, S.; Methia, M.; Khadimallah, M.A. Investigation of displacements and stresses in thick-walled FGM cylinder subjected to thermo-mechanical loadings. *Int. J. Comput. Methods Eng. Sci. Mech.* **2020**, *22*, 138–149. [CrossRef]
36. Gupta, V.; Kumar, V.; Ray, S. Modeling creep in a rotating disc with linear and quadratic composition gradients. *Eng. Comput.* **2009**, *26*, 400–421. [CrossRef]
37. Nie, G.; Zhong, Z.; Batra, R. Material tailoring for functionally graded hollow cylinders and spheres. *Compos. Sci. Technol.* **2011**, *71*, 666–673. [CrossRef]
38. Ansys®. *Academic Research Mechanical, Release 18.1, Help System, Coupled Field Analysis Guide, Help System, Mechanical APDL, Theory Reference*; ANSYS, Inc.: Canonsburg, PA, USA. Available online: https://www.ansys.com/academic/terms-and-conditions (accessed on 9 February 2013).

39. Jin-Feng, Z.; Wang, F.; Wei, A. A semi-analytical solution for shallow tunnels with radius-iterative-approach in semi-infinite space. *Appl. Math. Model.* **2019**, *73*, 285–302. [CrossRef]
40. Feng, G.; Zhu, C.; Wang, X.; Tang, S. Thermal effects on prediction accuracy of dense granite mechanical behaviors using modified maximum tangential stress criterion. *J. Rock Mech. Geotech. Eng.* **2023**, *15*, 1734–1748. [CrossRef]
41. Lyu, F.; Li, Y.; Huang, X.; Shi, Z.; Zeng, Y.; Lin, J. An investigation of creep age forming of AA7B04 stiffened plates: Experiment and FE modelling. *J. Manuf. Process.* **2019**, *37*, 232–241. [CrossRef]
42. Eggers, F.; Almeida Jr, J.H.S.; Lisbôa, T.V.; Amico, S.C. Creep and Residual Properties of Filament-Wound Composite Rings under Radial Compression in Harsh Environments. *Polymers* **2020**, *13*, 33. [CrossRef]
43. Dharmendra, C.; Rao, K.P.; Suresh, K.; Hort, N. Hot Deformation Behavior and Processing Map of Mg-3Sn-2Ca-0.4Al-0.4Zn Alloy. *Metals* **2018**, *8*, 216. [CrossRef]

Disclaimer/Publisher's Note: The statements, opinions and data contained in all publications are solely those of the individual author(s) and contributor(s) and not of MDPI and/or the editor(s). MDPI and/or the editor(s) disclaim responsibility for any injury to people or property resulting from any ideas, methods, instructions or products referred to in the content.